Photoabsorption spectra of solid O_2 in ultraviolet and far-vacuum ultraviolet region at 9–30 K

Jen-Iu Lo,[1] Hsiao-Chi Lu [ORCID],[1] Wei-Hsiu Hung,[2] B. Sivaraman,[3] N. J. Mason[4] and Bing-Ming Cheng [ORCID][1,5]⋆

[1]*Department of Medical Research, Hualien Tzu Chi Hospital, Buddhist Tzu Chi Medical Foundation, No. 707, Sec. 3, Chung-Yang Rd., Hualien City 970, Taiwan*
[2]*Department of Chemistry, National Taiwan Normal University, Taipei 116, Taiwan*
[3]*Physical Research Laboratory, Ahmedabad,380 009, India*
[4]*Centre for Astrophysics and Planetary Science, School of Physics and Astronomy, University of Kent, Canterbury, CT2 7NH, UK*
[5]*Tzu-Chi University of Science and Technology, No. 880, Sec. 2, Chien-kuo Rd., Hualien City 970, Taiwan*

ABSTRACT

We report ultraviolet and far-vacuum ultraviolet (FUV) absorption spectra of solid molecular oxygen recorded over the wavelength region 110–365 nm for temperatures between 9 and 30 K, in which the light source was dispersed from a synchrotron. The UV/FUV spectra of solids O_2 deposited at various temperatures appeared distinctly different profiles due to variation of compositions of α-O_2, β-O_2, and the imperfect crystal structure at the specific temperature; in addition, the icy sample exhibited its own scattering curve deposited at specific temperature. Resolved from the thermal ramping technique, the absorption spectra of solids α-O_2 and β-O_2 were established in the wavelength region 110–250 nm at 9 and 30 K, respectively, for the first time.

Key words: molecular data – ISM: molecules – methods: laboratory: molecular – methods: laboratory: solid state – ultraviolet: ISM.

INTRODUCTION

Molecular oxygen, O_2, is one of the most important chemical species in astrochemistry and astrobiology, both due to its anticipated role in the synthesis of more complex species and as a potential biomarker for photosynthetic-derived life. Accordingly, the search for O_2 in different regions of space continues to be an active research area. To date, O_2 has been observed in the molecular cloud ρ Ophiuchi (Larsson et al. 2007), in the interstellar medium (ISM) of Orion (Goldsmith et al. 2011), and in the protostar IRAS 16293–2422 B (Taquet et. al. 2018). In addition, the ROSINA-DFMS mass spectrometer on board the Rosetta spacecraft identified O_2 in the coma of comet 67P/Churyumov–Gerasimenko (Bieler et al. 2015).

In space, O_2 may exist in various phases depending upon the physical conditions within which it is found. O_2 in the solid (ice) phases has been studied in the laboratory (Johnson & Jesser 1997; Cooper, Johnson & Quickenden 2003) and has been shown to have six crystalline phases (Freiman & Jodl 2004) created under different temperature and pressure condtions. At the very low pressures, typical of the ISM, the α- and β-phases are expected to be formed. The α-phase is expected below 23.8 K and has a monoclinic crystal structure, while the β-phase is expected to form below 43.8 K with a rhombohedral crystal structure. The photoabsorption spectrum of each phase may provide a distinctive 'fingerprint' for each phase that can be used to identify the temperature of such ices in remote observations. Although the spectra of solid oxygen have

been extensively studied in the IR region (Smith, Keller & Johnston 1950; St. Louis & Crawford Jr. 1962; Cairns & Pimentel 1965; Minenko et al. 2000; Lo et al. 2022, 2023b) and in the visible region (Landau, Allin & Welsh 1962; Lo et al. 2022, 2023a, 2023b), the far-vacuum ultraviolet region (FUV) spectra of α, β-oxygen remains to be characterized (Lu et al. 2008, 2010).

In this work, we extend our previous work investigating the mid-IR, near-IR, and visible spectra of O_2 ice to shorter wavelengths (110 nm) in the FUV region. In the laboratory, the α-O_2 and β-O_2 phases usually co-exist in icy mixtures at low temperatures, such that, to date, no isolated FUV absorption spectra for the α- and β-O_2 phases have been reported yet. Therefore, in this work we aimed to resolve the FUV absorption of solids α- and β-O_2.

EXPERIMENTAL APPARATUS

The apparatus has been described in detail previously (Lu et al., 2005; Chou et al., 2014), so only the most salient features are described here. UV/FUV absorption spectra of solid O_2 were recorded in the UV and FUV regions from 365 to 110 nm using beamline 03 (BL03) on the Taiwan Light Source (TLS) at the National Synchrotron Radiation Research Center (NSRRC) in Taiwan. The BL03 beamline has a cylindrical-grating monochromator (CGM, 6 m) complete with four gratings; in this work, a grating with 450l/mm was selected to provide light over the wavelength range 100–365 nm. To monitor the intensity of the UV/FUV light from the grating, the dispersed light was passed through a 90 per cent transmitting gold mesh and recorded with an electrometer (Keithley 6512); subsequently, the transmitted light passed through a LiF window acting as a harmonic filter. The
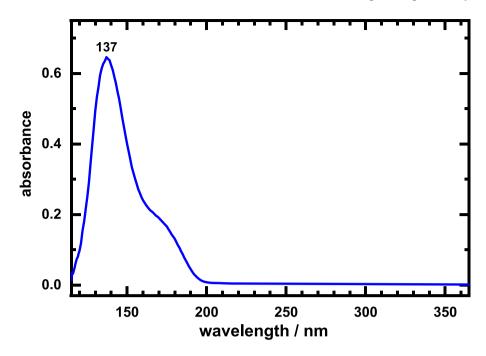
Figure 1. Absorption spectrum of O$_2$ ice deposited at 9 K over the wavelength range 115–365 nm.

dispersed radiation was incident on O$_2$ icy samples, deposited upon a LiF window substrate, with the beam being of nearly rectangular cross-section, $\sim$8 $\times$ 5 mm^2, and a mean flux 2 $\times$ 10^{11} photons s^{-1}. After passing through the ice film and substrate, the transmitted light impinged upon a glass window coated with sodium salicylate, the fluorescence from which was recorded with a photomultiplier (Hamamatsu R943) operated in a photon-counting mode.

Transmission spectra were recorded without and with icy samples with a typical spectral resolution of 0.2 nm. The photoabsorption spectra were then derived in absorbance units; the absorbance $= -$log (transmission) $= -$log (I/I_o), where I and I_0 are the intensities of the transmitted light with and without icy samples, respectively.

The ice samples were formed by depositing high (99.999 per cent) purity gaseous O$_2$ passed through a coil cold trap immersed in a liquid-nitrogen bath to remove any contaminants and nascent water, onto the LiF window attached to a rotary cryostat (APD HC-DE204S), which could be cooled to as low as 9 K. The temperature of the sample was regulated by a temperature controller (Lake Shore 340) with the ice being heated or cooled at a rate of 1 K min^{-1}.

The gaseous O$_2$ was obtained from Matheson with a nominal purity 99.999 per cent.

RESULTS AND DISCUSSION

The lowest temperature that could be maintained by the cryostat for the measurement of the photoabsorption of the O$_2$ ice sample was 9 K, Fig. 1 shows the photoabsorption spectra for O$_2$ ice between 115 and 365 nm at 9 K. As in our previous work (Lu et al. 2008; Sivaraman et al. 2014; Chou et al. 2018) a broad-band is located between 115–200 nm with a strong peak at about 137 nm and a shoulder near 173 nm in the UV/FUV region. Beyond 200 nm, the absorption is weak and becomes monotonously faint to 365 nm. For this reason, we performed the measurements with thicker samples to study the wavelength region greater than 200 nm, we then normalized the overlapping regions to produce the absorption curve as shown in Fig. 1.

In comparison with gas-phase photoabsorption spectra, O$_2$ in the FUV and near regions is expected to reveal the Herzberg continuum between 200 and 242 nm, the Schumann–Runge bands between 175 and 200 nm, the Schumann–Runge continuum between 130 and 175 nm, excitation to the state E $^3\Sigma_u^-$ at 124.4 nm, and the a $^1\Delta_g$ state at 120.5 nm (Metzger & Cook 1964; Hudson, Carter & Stein 1966; Huffman 1969; Ogawa & Ogawa 1975; Gibson et al. 1983; Wang et al. 1987; Yoshino et al. 2005; Lu et al. 2010 and references there in). In the FUV region, the photoabsorption spectra of gaseous O$_2$ consists of both discrete lines and continuum bands; whereas, the absorption of solid O$_2$ ice formed at 9 K has shown a continuum profile with a maximum at 137 nm and a shoulder near 173 nm.

Previous work (Lo et al. 2022, 2023a, 2023b) using the end-station at beamline BL21A2 at TLS measured absorption spectra of solid O$_2$ in the near IR, visible and ultraviolet regions. Combining the data in Fig. 1 with this earlier data, we have created the composite spectrum shown in Fig. 2, which displays the resultant absorption curve of O$_2$ ice deposited at 9 K in the wavelength region 115–1020 nm. Due to great variation in the absorption cross-sections, we present the absorption on a log scale. The strong absorption of O$_2$ ice in the FUV region is about two orders greater than that in the UV region, and the latter is almost two orders higher than that in the visible and near IR regions.

Fig. 2 also shows a strong fringe pattern in the wavelength region between 650 and 1020 nm. These fringes occur because of interference due to the thickness of the solid O$_2$ ice. The separations of the fringes have values between 301 and 305 cm^{-1}. Two factors affect the separation of the fringes; the refractive index and the thickness of the icy samples. If we assume the refractive index of solid O$_2$ to be 1.30 (Rocha & Pilling 2014), we can derive the thickness of the icy O$_2$ to be 12.2 $\pm$ 0.2 μm (Lo et al. 2023b). Based on the value of this thickness and that the strong absorption band is 1/600 in FUV region, we estimate the thickness of the O$_2$ ice in the present UV/FUV studies to be 20 $\pm$ 5 nm.

As indicated in our previous work, the intensities and profiles of IR, near-IR, and visible spectra of solid O$_2$ depend strongly on the
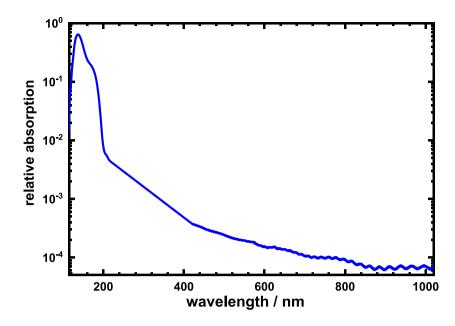
Figure 2. Absorption spectrum of O_2 ice deposited at 9–10 K over the wavelength range 115–1020 nm. The curve in the region 350–1050 nm is adapted from Lo et al. 2022 and 2023.

deposition temperature of the icy samples therefore we studied the spectra of solid O_2 at shorter wavelengths in FUV region. Fig. 3 displays the absorption spectra of O_2 ice deposited at 10, 15, 18, 21, 24, 27, 30, and 32 K, respectively, in the wavelength region 114–350 nm. The triple point of O_2 is 54.36 K; thus, it is possible for O_2 to exist as an ice below 54 K. However, the existence of solid O_2 at low temperature is dependent on the experimental conditions and systems in laboratory, especially the cooling power of the cryostat and the conductance of the pumping system (Bennett & Kaiser 2005). In this work, we obtained no absorption of solid O_2 for samples deposited at 32 K, as shown in Fig. 3 (h); hence, we could only record the spectra of O_2 ices in the temperature range 9–30 K in this work.

In Fig. 3, each spectral curve of O_2 ice at a specific temperature was measured with different thicknesses of samples to ensure similar absorbance. In the strong absorption region wavelength region (shorter than 200 nm), thin O_2 ices were used with thicknesses estimated about 20–30 nm whereas to improve the signal to noise ratios for the weak absorption at longer wavelengths, thicker O_2 ices, as much as 2 μm, were used. All the spectra were normalized using values intergrated in the wavenumber region 87 720–40 000 cm^{-1}, 114–250 nm, with the assumption that the corresponding oscillator strengths are the same for O_2 ices deposited at temperatures between 10 and 30 K. By these means, we derived the absorption spectra of O_2 ices deposited at the different temperatures as shown in Fig. 3. Notably, Fig. 3 (h) exhibits almost no residue curve; this result hints that the O_2 sample contains no detectable impurity. Also, as proven from the previous IR spectra, the solids O_2 possessed no detectable H_2O, CO_2, and other impurity existed in the icy samples (Lo et al. 2022); so that, the target ices with implemented special precautions could remove the possible contaminants in O_2 ices. Consequently, the alteration of the spectral features in these spectra are associated only with different structural compositions for molecular oxygen at various temperatures.

A significant change in the photoabsorption spectrum is seen as the temperature increases with the emergence of a strong second peak above 170 nm at temperatures above 21 K, a peak that shifts to higher wavelengths as the temperature increases to 30 K. In order

to understand the presence of this second peak, we can reference changes in the IR spectra over the same temperature range (Lo et al. 2022, 2023b). According to previous work, solid α-O_2, the imperfect (amorphous) structure of O_2 ice, and solid β-O_2 can exist at the deposited temperatures $\leq$24, $\leq$27 K, and between 24–30 K. Thus, the O_2 ices might contain compositions of solids α-O_2, β-O_2, and the imperfect (amorphous) structure at different deposited temperatures below 30 K. We suggest that the spectral curves shown in Figs 3(a), (b), (c), and (d) deposited at 10, 15, 18, and 21 K, respectively, might constitute absorption data of the solid α-O_2 and the imperfect (amorphous) structure of O_2 ice, in which, the imperfect O_2 lattice occurred most strongly at 10 K and became weaker at higher temperatures. Considering that the absorption band 137 nm was the most intense at the deposited temperature 10 K and appeared to decrease at higher deposited temperatures, we assume that the 137 nm band might be associated with the presence of the imperfect O_2 lattice; whereas, the shoulder near 173 nm might arise from the solid α-O_2.

At the phase transition temperature, 24 K, the deposited solid sample could contain the α-O_2, the imperfect lattice ice and in addition solid β-O_2. At 27 K, the O_2 ice consists of the imperfect lattice and the solid β-O_2 without the α-O_2; the resultant absorption curve is displayed as Fig. 3(f). At 30 K, the icy sample possesses only the solid β-O_2, whose absorption spectrum is shown in Fig. 3(g), with the maximum band at about 185 nm and the broader band near 140 nm.

It should be noted that the absorption curves possess long tails beyond 195 nm at deposition temperatures above 24 K. These might be due to strong light scattering effects at higher deposition temperatures. In order to remove these effects and present pure ice photoabsorption spectra, we deposited O_2 at 9 K and then warmed up the substrate to 30 K, Fig. 4(a). This spectrum has a much reduced tail in the long wavelength region compared to Fig. 3(f). We therefore conclude that Fig. 4(a) can represent the UV/FUV absorption spectrum of the solid β-O_2 at 30 K; its absorption bands are at 144 and 166 nm. Next, we re-cooled the icy sample to 9 K and obtained the spectrum at 9 K as displayed in Fig. 4(b), which
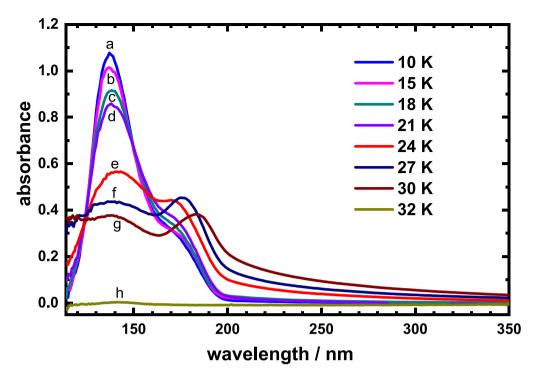
Figure 3. Absorption spectra of O_2 ice deposited at (a) 10, (b) 15, (c) 18, (d) 21, (e) 24, (f) 27, (g) 30 and (h) 32 K over the wavelength region 114–350 nm.
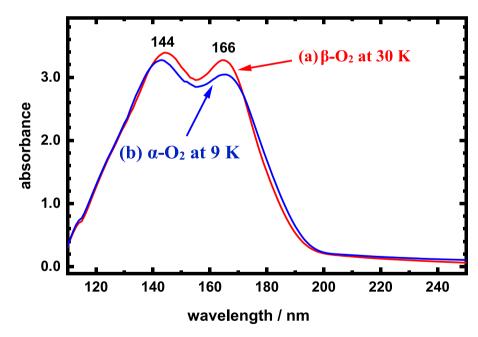

Figure 4. Absorption spectra of O_2 ice over the wavelength region 110–250 nm, deposited at 9 K then, (a) warmed to 30 K and (b) re-cooled to 9 K

represents the UV/VUV absorption spectrum for the solid α-O_2 at 9 K. The UV/VUV absorption spectra for both solids α- and β-O_2 appear very similar in their profiles.

To confirm the characteristic spectra for these solid phases, we warmed up a 9 K ice to 30 K and re-cooled down to 9 K, hence we repeatedly recorded spectra from the solid β-O_2 at 30 K and the solid α-O_2 at 9 K as displayed in Figs 5(a) and (b), respectively. The UV/VUV absorption curves in Figs 4 and 5 for α- and β-O_2 agree within expected experimental errors, and therefore we believe that the obtained spectra are representative of these two solid phases.

Using our previous data in the visible, near-IR and IR regions, we create absorption spectra for solid O_2 over the wavelength range between 110 and 20 000 nm, Fig. 6. Overall, the absorption of α- and β-O_2 are similar over this extended wavelength region 110–20 000 nm; but are different from the solid O_2 deposited at 9 K. Fig. 6 can provide semiquantitative information of absorptions for solids α- and β-O_2 in the wavelength range 110–20 000 nm; for example, the absorptions of solids α- and β-O_2 in the FUV region are at least three to four orders of magnitude greater than those in the IR region.
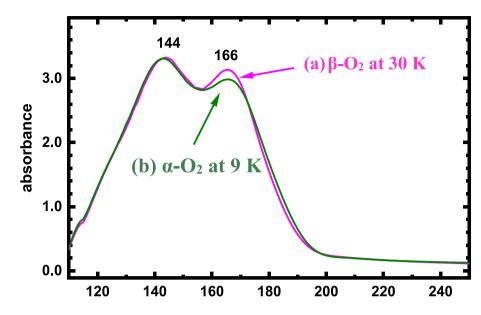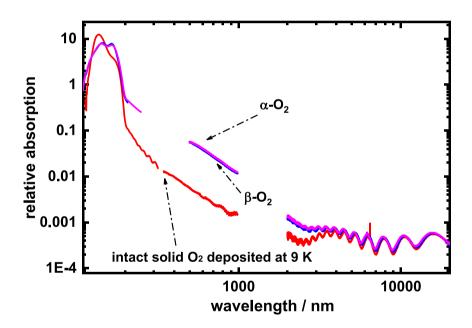
Figure 5. Absorption spectra of O_2 ice in the wavelength region 110–250 nm, deposited at 9 K, warmed to 30 K, and re-cooled to 9 K then (a) warmed to 30 K again and (b) re-cooled to 9 K again.

Figure 6. Relative absorption spectra of solid α-O_2 at 9 K, solid β-O_2 at 30 K, and O_2 deposited at 9 K in wavelength ranges 110–250, 450–1020, and 2000–20 000 nm (5000–500 cm^{-1}). Note: there is no data for α- and β-O_2 in the wavelength range 250–450 nm and 1020–2000 nm.

CONCLUSIONS AND RELEVANCE TO ASTROCHEMISTRY

The absorption spectra of O_2 ices over the UV/FUV wavelength range 110–350 nm for temperatures between temperatures 9 and 30 K have been measured. Spectra show the presence of both α-O_2 and β-O_2 ice as well as imperfect/amorphous ice. Through a heating/cooling (annealing) cycle, the individual spectra of α-O_2 and β-O_2 ice were determined and found to be very similar.

These results have consequences for astronomy and planetary science. Irradiation of O_2 ice by energetic FUV light may trigger chemical reactions to form complicated astronomical molecules, and that may play a key in the prebiotic chemistry leading to the origin of

life in space (Ward et al. 2019). The different photoabsorption spectra for α-O_2, β-O_2, and amorphous ice will result in different O atom yields, which, in turn, may affect chemical pathways and rates. We thus suggest that the previous work on the chemistry of irradiated solid O_2 (Ennis & Kaiser 2012; Sivaraman et al. 2014; Zhen & Linnartz 2014; Chou et al. 2018; Lo et al. 2018a, 2018b; Leroux & Krim 2021) be revisted to determrine the role of photoabsorption in different O_2 ice phases.

NOTES

DATA AVAILABILITY

All data discussed in the paper will be made available to readers on request to the corresponding author.

REFERENCES

Bennett C. J., Kaiser R. I., 2005, ApJ, 635, 1362
Bieler A. et al., 2015, Nature, 526, 678
Cairns B. R., Pimentel G. C., 1965, J. Chem. Phys., 43, 3432
Chou S.-L., Lo J.-I., Lin M.-Y., Peng Y.-C., Lu H.-C., Cheng B.-M., 2014, Angew. Chem. Int. Ed., 53, 738
Chou S.-L., Lo J.-I., Peng Y.-C., Lu H.-C., Cheng B.-M., Ogilvie J. F., 2018, Phys. Chem. Chem. Phys., 20, 7730
Cooper P. D., Johnson R. E., Quickenden T. I., 2003, Planet. Space Sci., 51, 183
Ennis C., Kaiser R. I., 2012, ApJ, 745, 103
Freiman Y. A., Jodl H. J., 2004, Phys. Rep., 401, 1
Gibson S. T., Gies H. P. F., Blake A. J., McCoy D. G., Rogers P. J., 1983, J. Quant. Spectrosc. Radiat. Transfer, 30, 385
Goldsmith P. F. et al., 2011, ApJ, 737, 96
Hudson R. D., Carter V. L., Stein J. A., 1966, J. Geophys. Res., 71, 2295
Huffman R. E., 1969, Can. J. Chem., 47, 1823
Johnson R. E., Jesser W. A., 1997, ApJ, 480, L79
Landau A., Allin E. J., Welsh H. L., 1962, Spectrochim. Acta, 18, 1–19
Larsson B. et al., 2007, A&A, 466, 999
Leroux K., Krim L., 2021, MNRAS, 500, 1188
Lo J.-I., Chou S.-L., Peng Y.-C., Lu H.-C., Ogilvie J. F., Cheng B.-M., 2018a, ApJ, 864, 95
Lo J.-I., Chou S.-L., Peng Y.-C., Lu H.-C., Ogilvie J. F., Cheng B.-M., 2018b, Phys. Chem. Chem. Phys., 20, 13113
Lo J.-I., Lu H.-C., Hung W.-H., Cheng B.-M., 2023a, MNRAS, 519, 3879
Lo J.-I., Lu H.-C., Hung W.-H., Ogilvie J. F., Cheng B.-M., 2023b, MNRAS, 522, 3183
Lo J.-I., Lu H.-C., W.-H. O. J. F., Cheng B.-M., 2022, MNRAS, 514, 2815
Lu H.-C., Chen H.-K., Chen H.-F., Cheng B.-M., Ogilvie J. F., 2010, A&A, A520, A19
Lu H.-C., Chen H.-K., Cheng B.-M., Kuo Y.-P., Ogilvie J. F., 2005, J. Phys. B: At. Mol. Opt. Phys., 38, 3693
Lu H.-C., Chen H.-K., Cheng B.-M., Ogilvie J. F., 2008, Spectrochimica Acta A Mol. Biom. Spectr., 71, 1485
Metzger P. H., Cook G. R., 1964, J. Quant. Spectrosc. Radiat. Transfer, 4, 107
Minenko M., Vetter M., Brodyanski A. P., Jodl H., 2000, Fiz. Nizk. Temp., 26, 647
Ogawa S., Ogawa M., 1975, Can. J. Phys., 53, 1845
Rocha W. R. M., Pilling S., 2014, Spectr. Acta Part A: Molecul. Biomelecul. Spectr., 123, 436
Sivaraman B., Nair B. G., Sekhar B. N. R., Lo J.- I., Sridharan B., Cheng B.-M., Mason N. J., 2014, Chem. Phys. Lett., 603, 33
Smith A. L., Keller W. E., Johnston H. I., 1950, Phys. Review, 79, 728
St. Louis R. V., Crawford B., Jr., 1962, J. Chern. Phys., 37, 2156
Taquet V. et al., 2018, A&A, 618, A11
Wang J., McCoy D. G., Blake A. J., Torop L., 1987, J. Quant. Spectrosc. Radiat. Transfer, 38, 19
Ward L. M., Stamenković V., Hand K., Fischer W. W., 2019, Astrobiology, 19, 811
Yoshino K., Parkinson W. H., Ito K., Matsui T., 2005, J. Mol. Spect., 229, 238
Zhen J., Linnartz H., 2014, MNRAS, 437, 3190

This paper has been typeset from a Microsoft Word file prepared by the author.